Numerical Simulation of Transpiration Cooling on Stagnation Line in Thermochemical Non-Equilibrium

Samuel Brody *, Kin Sing Lau †, Justin Clarke ‡, Matthew McGilvary § Luca Di Mare ¶
Oxford Thermofluids Institute, University of Oxford, Oxford, Oxfordshire, OX1 2JD

Sharp leading edges offer drag and maneuverability advantages for hypersonic applications such as powered flight and some gliding trajectories. The reduction in standoff distance resulting from the adoption of sharp edges, however, results in increased surface convective heating that needs to be managed. Ablative layers are unfeasible as a cooling strategy for sharp edges, because they lead to a change in surface curvature radius and render systems non-reusable. Among possible strategies, transpiration cooling has been presented as an attractive option in terms of cooling effectiveness and system complexity. In this study, a method is presented for the numerical simulation of transpiration cooling in proximity of the stagnation point of sharp leading edges or tips. The method is suited to both equilibrium and non-equilibrium flight regimes and is based on stagnation line theory presented by Cheng. Transport properties are determined through rigorous Chapman-Enskog theory. Non-equilibrium cases are handled with Park's two temperature model. The solver explicitly represents coolant flow through a porous medium. Detailed temperature profiles and mole fractions in the shock layer and within the porous medium can be evaluated, with variations in in these profiles computed as functions of flight altitude, speed, leading edge radius, and coolant flow rate and composition. Argon, helium, and nitrogen are tested for their efficacy. The ability of different coolant mixtures to limit the transport of catalytic species to the surface is studied.

Nomenclature

$\dot{w}_{i/s}$	=	Mass rate of production of species *i/s*
$\vec{q}$	=	Vector of fluid properties
D	=	Coefficient of diffusion
H	=	Total enthalpy
h	=	Enthalpy
H_v	=	Volumetric heat transfer coefficient
$k_{b,r}$	=	Backward reaction rate coefficient for reaction r
$k_{f,r}$	=	Forward reaction rate coefficient for reaction r
M_i	=	Molar mass of species i
n	=	Molality
NS	=	Number of species in gas mixture
p	=	Pressure

*DPhil Candidate, Department of Engineering Science, Oxford Thermofluids Institute, University of Oxford.
†MEng, Department of Engineering Science, Oxford Thermofluids Institute, University of Oxford.
‡DPhil Candidate, Department of Engineering Science, Oxford Thermofluids Institute, University of Oxford.
§Professor, Oxford Thermofluids Institute, Department of Engineering Science, University of Oxford.
¶Associate Professor, Oxford Thermofluids Institute, Department of Engineering Science, University of Oxford.

$R_{b,r}$ = Backward reaction rate for reaction r

$R_{f,r}$ = Forward reaction rate for reaction r

T = Temperature

u = Streamwise velocity component

v = Wall-normal velocity component

w = Span-wise velocity component

X_i = Molar concentration of species i

α = Darcy penalization term

$\alpha_{i,r}$ = Stoichiometric coefficient of reactant i in reaction r

$\beta_{i,r}$ = Stoichiometric coefficient of reactant i in reaction r

δ = Thickness of the viscous shock layer

δ_p = Distance of plenum to interface

λ = Thermal conductivity

μ = Dynamic viscosity

ρ = density

σ = electrical conductivity

σ_{SB} = Stefan-Boltzmann Constant

τ = Shear stress tensor

ε = porosity, emissivity

∞ = Free-stream conditions

e = Electron-vibrational.

n = Normal

s = Species/Solid

t = Translational-rotational.

PNS = Parabolized Navier-Stokes

TC = Transpiration Cooling

I. Introduction

Hypersonic flight has received increased attention in recent years for both civil and defense applications. In both contexts, considerations of aerodynamic performance and maneuverability indicate that sharp leading edges are advantageous. A sharp leading edge results in a reduced standoff distance, leading to a thinner shock layer and increased surface convective heat flux. This heat flux can be over 1 MW/m^2, requiring an active cooling technology rather than passive reradiation. Ablative layers are not a feasible mitigation strategy for sharp leading edges, because they are not reusable and invariably result in a radius of curvature that grows during flight, thereby negating the advantages of the initial choice of a sharp geometry.

Transpiration cooling (TC) has been presented as a favorable compromise between effectiveness and system complexity. TC operates by injecting a coolant through a porous patch of the surface that requires cooling. TC cools the surface by 1) convection of a relatively cold coolant through the porous layer; 2) displacing the hot external stream in proximity of the surface and reducing the temperature gradient; 3) inhibiting surface reactions which contribute to the overall heat flux [1]. According the selection of the coolant mixture, TC can also be beneficial as an oxidation management method, as it can displace oxygen away from the surface. TC requires the provision of a feed system that needs to be compatible with the limited amount of space available behind the surface to be cooled. Typically, this can be achieved by concealing a plenum behind the edge to be cooled and moving the plumbing where thermomechanical and spatial arrangement constraints are less taxing. The performance of a TC system depends on the hydraulic properties of the porous layer, the coolant mass flux density, and its feed conditions.

An ideal system should operate with the lowest possible plenum pressure to reduce stress and with the lowest possible coolant flow rate. To minimize tank storage, it is desirable that the cooled surface be uniformly covered by the coolant stream. However, it is undesirable to inject excess coolant. While drag has been shown to change only slightly [2], risk of boundary layer blowoff may reduce the aerodynamic advantages of a sharp leading edge. Performance data on transpiration cooling devices in hypersonic environments have been obtained for a range of applications, including stagnation line heating [1]. Testing of cooling devices is however limited in scope because of the difficulty of either achieving realistic free stream enthalpies or Reynolds numbers or of obtaining data at realistic surface temperatures in transient facilities. Further, the large expense of flight tests is often prohibitive. Therefore, there is an acute need for engineering tools to perform accurate but expeditious calculations on transpiration cooling systems, their performance, and their effect on downstream aerodynamics.

Engineering calculations of transpiration cooling systems should be able to predict the pressure margin/mass flow rate characteristics of the system as well as the heat flux surface temperature reduction as functions of coolant mass flow rate, flight speed and attitude, altitude, and coolant composition. These data should be made available in a time compatible with design iterations and in presence of incomplete data on the vehicle geometry. The numerical prediction of transpiration cooling performance in a hypersonic environment is however complicated by: partially dissociated and ionized plasma, thermal and chemical non-equilibrium, surface catalysis, and radiation from the surface. Additionally, in a transpiration cooling simulation, the flow through the porous medium also needs to be modelled. This further complicates the simulation task, because it requires the coupling of the high-subsonic (and further downstream supersonic) shock layer with a nearly incompressible flow domain within the porous block and with a conduction problem through the block material. It is clear that the complete numerical simulation of a transpiration cooled vehicle is a formidable challenge. This challenge however, is not strictly needed for engineering calculations, because the heat flux - and presumably the coolant consumption rate - scale with the condition at the stagnation points/line where a vehicle experiences the most intense heating.

Efficient methods for calculation in proximity of stagnation points/lines have been known for several years. Stagnation line theory developed by Blottner[3] as a continuation of Cheng's thin shock layer work [4] can be harnessed to characterize the local geometry of a sharp leading edge vehicle. Thus, the combination of computational expediency with physical realism within the area in proximity of the stagnation point provides the framework for an accurate engineering tool for the application of transpiration cooling to hypersonic sharp leading edges. The contribution of this paper is the coupling of the entire domain (shock layer and porous medium). This allows for the accurate description of the porous interface. The solver is very efficient due to the simplification of the complex TC problem, while maintaining accuracy to the most prominent aspects of the problem. The paper is organized into four additional sections. Section II describes the formulation of the method. Section III presents validation of the solver against correlations and previous results. Section IV presents results on the following topics:

- sensitivity of surface temperature and compositions for a specific flight altitude and speed for a variety of coolant injection rates and compositions
- detailed profiles of species and temperatures through the stagnation line for the selected case

Section V presents conclusions on the results and discussion of pathways for future work.

II. Methodology

A. Parabolized Navier Stokes

The method presented in this paper employs the parabolized Navier Stokes (PNS) equations due to their ability to preserve the full thermochemical model at a low computational cost. This paper considers flow regimes likely experienced by hypersonic vehicles: low free-stream density and high flight velocity. In these regimes, shock transition occurs over a layer of non-negligible thickness and Reynolds numbers remain low enough to allow an assumption of laminar flow in the regions of interest around the stagnation point. Gnoffo's [5] presentation of the conservation equations for hypersonic flows in thermochemical nonequilibrium is used as the basis for the governing equations employed in this paper. Further details can be found in [6].

$$0 = -\nabla \cdot (\rho_s \vec{u}) - \nabla \cdot (\rho_s D_s \nabla y_s) + \dot{w}_s \tag{1}$$

$$0 = -\nabla \cdot (\rho \vec{u} \otimes \vec{u}) - \nabla p + \nabla \cdot \tau - \alpha \frac{\mu}{k_D} \vec{u} \tag{2}$$

$$0 = -\nabla \cdot (\rho e_v \vec{u}) + \nabla \cdot ((k_e + k_v) \nabla T_v) + \nabla \cdot \left(\sum_{s=1}^{n_s} h_{v,s} (\rho_s D_s \nabla y_s) \right) - p_e \nabla \cdot \vec{u} - Q \tag{3}$$

$$0 = -\nabla \cdot (\rho H \vec{u}) + \nabla \cdot q_c + \nabla \cdot q_d + \nabla \cdot (\tau \cdot \vec{u}) - H_v (T_s - T_t) \tag{4}$$

The mass production rate, $\dot{w}_s$, and the radiation loss term, Q are taken directly from Gnoffo. The conductive heat flux, q_c, and diffusive enthalpy flux, q_d, are defined using Fourier's law and Fick's law, respectively. The viscous stress term τ is defined:

$$\boldsymbol{\tau} = \mu \left(\nabla \boldsymbol{u} + (\nabla \boldsymbol{u})^T - \frac{2}{3} (\nabla \cdot \boldsymbol{u}) \right) \tag{5}$$

A Darcy penalization has been included in the momentum equation as the final term [7]. The constant α is zero when in the boundary layer and one in the porous medium. k_D is a material property term describing the permeability of the porous medium. This property can be attained through experiment or predicted based on pore size and porosity [8]. Further, a solid energy equation is required, comprising a convection term and a solid-fluid heat exchange term [9]. The latter is also included in the total energy equation.

$$0 = k_s (1 - \varepsilon) \nabla \cdot \left(\frac{\partial T_s}{\partial dy} \right) + H_v (T_s - T_t) \tag{6}$$

For the purpose of this study, the governing equations are cast in spherical coordinates but could similarly be employed in cylindrical coordinates for applications to leading edges. Coupled with Cheng's analysis, a modified form of the Rankine-Hugoniot relations can be generated stating the conservation of mass, momentum, species, and enthalpy fluxes across the shock interface layer, including viscous fluxes at the shock interface. The modified Rankine-Hugoniot relations can be used as boundary conditions for the shock layer once the shock interface location is fixed. While the current study employs this technique, the simulation could instead begin at the free stream with integration through the shock.

B. Stagnation Line Problem with Transpiration Cooling

The flow along the stagnation line can be determined independently from the flow around the rest of the body. The surface geometry only appears in the stagnation line equations through the radius of curvature of the surface and, for hypersonic flows, through the radius of curvature of the shock. Homann [10] presented a solution for the stagnation line in a viscous flow as a separation of variable problem, exploiting the known shape of the wall and of the stagnation streamline. Herring [11] presented a derivation for the equations ruling the flow near the stagnation point over a spherical cap based on a trigonometric expansion around the center-line.

In the present work, the stagnation line and a small volume of gas surrounding it are idealized as a one-dimensional flow path. For the purpose of representing the transpiring leading edge, the domain is extended into the porous medium.

Boundary conditions are applied at the shock surface via the Rankine-Hugoniot relations, and at the plenum, where coolant mass flow rate (or plenum pressure for a real system), temperature, and composition are assigned. The flow path

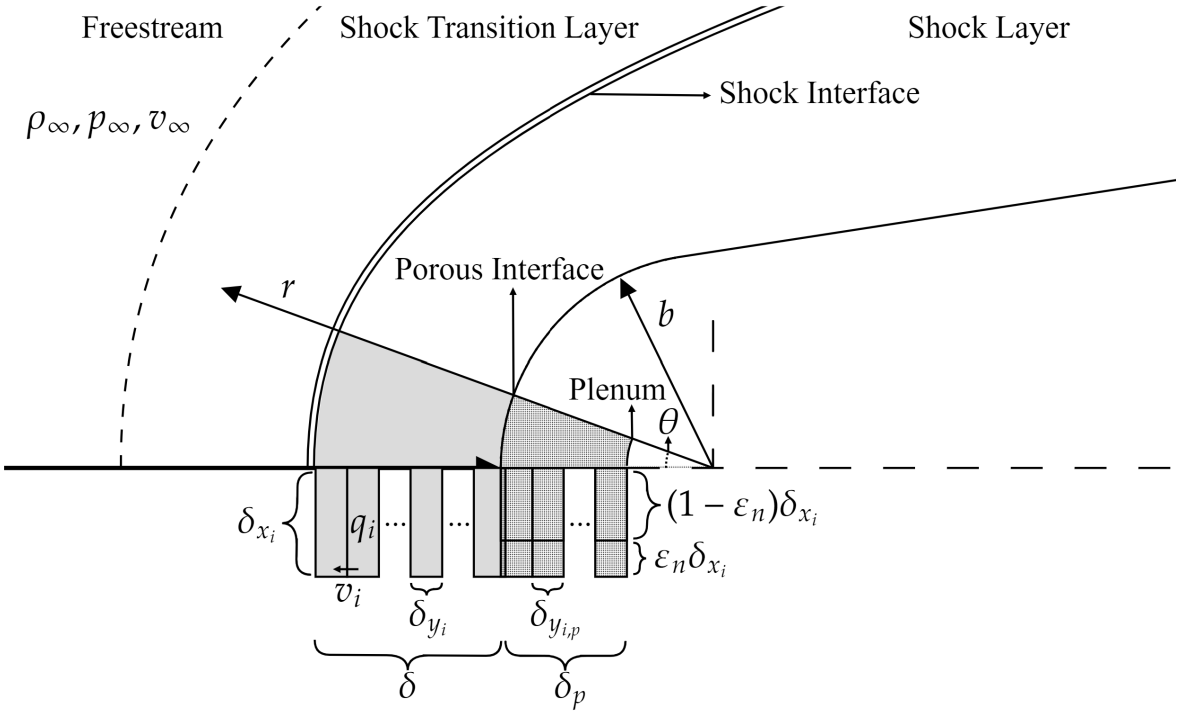

Fig. 1 Schematic of numerical setup of transpiration cooled leading edge stagnation line solver

is divided into control volumes, as depicted in Figure 1. The porous medium is treated as a homogeneous and possibly anisotropic phase characterized by a porosity tensor, a permeability, and a wet area per unit volume. Within the porous medium, an additional conservation equation is solved, which represents the energy balance for the solid phase.

Herring's derivation is based on constant properties, but the stagnation line problem can be formulated for reacting flow as well, both in equilibrium and non-equilibrium conditions. Because the momentum equation remains unchanged for a two temperature model, Herring's approximation for the relation between shock strength, curvature, and tangential pressure gradient holds rigorously for an infinitely thin shock. Fay and Riddell [12] presented a solution for the stagnation line problem in frozen and equilibrium dissociated flow. Blottner [3] calculated stagnation line solutions in non-equilibrium air using a 5-species mechanism. In the conditions of interest for this study, translational temperature and electron temperature can vary significantly. The development and implementation of a version of the solution method, applied to shock tube simulation, is presented by Clarke et. al [13]. For high-speed scenarios, a significant portion of the overall cooling make come passively through reradiation. In the solver, the reradiation flux from the surface to the surroundings is modelled using the Stefan-Boltzmann equation:

$$\dot{q}_{rad} = \varepsilon \sigma_{SB} T_s^4 \tag{7}$$

This passive cooling can be hindered by oxidation, emphasizing the importance of decreasing surface transport of oxidizing species [14]. Lastly, a fully-catalytic wall is assumed by enforcing mole fractions of zero for charged species [15].

C. Thermochemical Model

Hypersonics is complicated by the presence of non-equilibrium phenomena. Thus, the flow around a hypersonic vehicle is best modeled as a partially dissociated and partially ionized non-equilibrium plasma, with some level of ionization and slow rates of chemical reactions and thermal equlibrization relative to flow velocity. Park's two temperature model is implemented in this work, with translational and rotational modes evaluated at the translational temperature and electronic and vibrational modes evaluated at the electron temperature [16]. Transport properties are determined through Chapman-Enskog Theory, as presented by Hirschfelder et al. [17] but are adapted to the

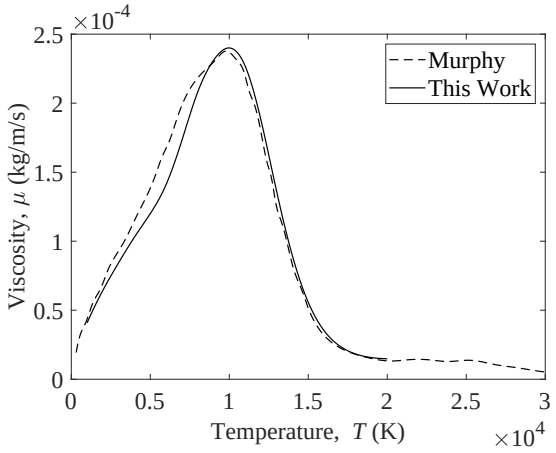

Fig. 2 Viscosity of nitrogen compared with data from Murphy [25]

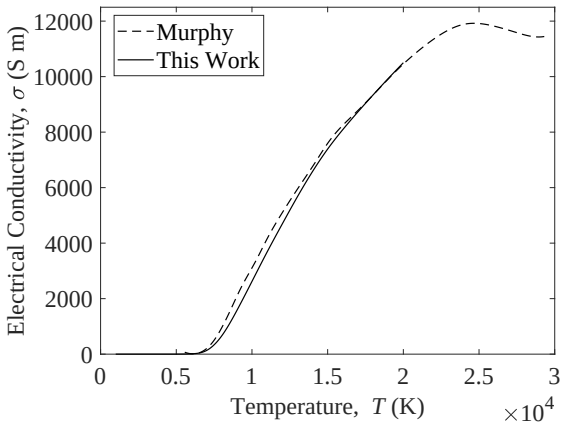

Fig. 3 Electrical conductivity of nitrogen compared with data from Murphy [25]

two-temperature framework. Collision integrals are computed using a range of potential functions and tabulations best suited for each species interaction. In computing transport properties, binary property terms are computed at the translational temperature for interactions involving only heavy particles, while the electron temperature is used for interactions involving electrons. An 11-species air model plus injectant is employed. Often, transport properties are computed using the mixing rules presented by Yos [18], as implemented in the work of Gupta [19] and Gnoffo[5]. These mixing rules offer low computational costs. Wilke [20] and Gordon and McBride [21] present similar mixing rules which were assessed by Palmer and Wright [22] to halve the computational cost relative to a full multi-component "rigorous" method, as presented by Hirschfelder et. al [17]. While computationally efficient, these evaluations can be inaccurate, with non-negligible error arising at temperatures above 10,000 K for air, where ionization effects begin to dominate, as shown by [22]. Capability to compute transport properties for the Park two-temperature model using rigorous kinetic theory has been developed by the University of Oxford Numerical Analysis Group and is implemented into the stagnation line solver for transpiration cooling. The use of rigorous modelling is especially important in the context of this study, as transpiration of light coolant gases requires accurate assessment of diffusion coefficients.

From several resources [17, 23, 24], semi-rigorous formulations implementing Park's two temperature model can be employed. Murphy presented an implementation of a multi-component rigorous method [25]. The methods for calculating transport properties in this work were validated against Murphy's work, with results presented in Figures 2-4. Further, Murphy presented a comparison between the viscosity of 11 species air, as computed with his rigorous method and Gupta's mixing rule. Again, the methods used in this work align nicely with Murphy's, as shown in Figure 5.

Reaction rates can be defined using the stoichiometric ration of each reaction [19]

$$\sum_{i=1}^{NS} \alpha_{i,r} X_i \underset{k_{f,r}}{\overset{k_{b,r}}{\rightleftharpoons}} \sum_{i=1}^{NS} \beta_{i,r} X_i \tag{8}$$

Moss [27] presents the production rates as:

$$\dot{w}_i = M_i \sum_{r=1}^{NS} (\beta_{i,r} - \alpha_{i,r})(R_{f,r} - R_{b,r}) \tag{9}$$

Reaction rates and coefficents are taken from Gnoffo's work [5].

$$R_{f,r} = k_{f,r} \prod_{j=1}^{NS} (\rho_j / M_j)^{\alpha^{j,r}} \tag{10}$$

$$R_{b,r} = k_{b,r} \prod_{j=1}^{NS} (\rho_j / M_j)^{\beta^{j,r}} \tag{11}$$

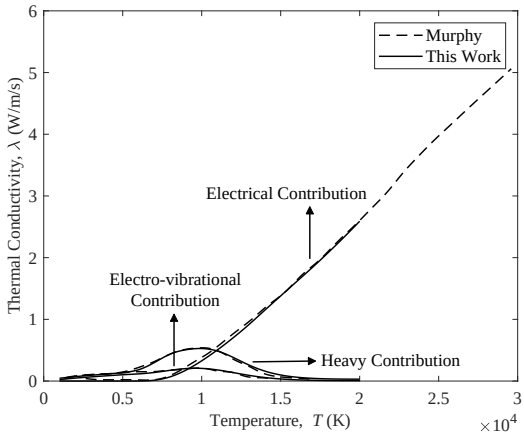

Fig. 4 Thermal conductivity of nitrogen compared with data from Murphy [25]

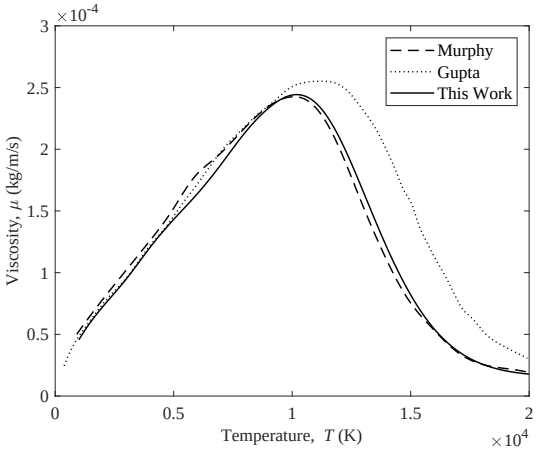

Fig. 5 Viscosity of air compared with data from Murphy [26] and Gupta [19]

Forward reaction rates are evaluated at the average of the electro-vibrational and translational temperature, whereas the backward reaction rates are evaluated at the translational temperature. Tables 1 and 2, included in the appendix, provide the reactions and reaction coefficients for a standard 11-species air model (with helium and argon added for use as injectants). Backward reaction rates can be determined from equilibrium constants using Gibbs free energy. However, the temperatures relevant in this study would not cause appreciable amounts of ionization in either argon or helium.

D. Numerical Method

The one-dimensional computational domain is discretized in cells. The conservation equations are solved in discrete form using a finite volume discretization. The solution process is complicated by two elements: variable flow directions and the presence of two interfaces. The first is at shock, and the second defines the surface. Variable flow direction presents challenges to numerical stability, as the Newton Raphson method in this solver generally employs first-order finite differencing. Thus, the system of equations must be discretized and solved using differencing schemes that preserve upwinding regardless of flow direction. This is accomplished using a staggered grid arrangement, as presented by Harlow and Welch [28]. Using this arrangement, displayed in Figure 6, normal velocity is defined at the interface with all other state variables defined at the cell center. Fluxes can then be defined such that information propagates upstream of the current flow direction at cell interfaces. Generically, the resulting system of equations can be solved using a block matrix scheme with a block tridiagonal Jacobian structure. The solution process recasts the system defined in Equations 1-6, $F(\vec{q}) = \vec{0}$, as the residuals of a perturbed flow state: $R(\partial(\vec{q})) = \vec{0}$.

$$\begin{bmatrix} a_{1,2} & a_{1,3} & \mathbf{0} & \dots & \mathbf{0} \\ a_{2,1} & a_{2,2} & a_{2,3} & \mathbf{0} & \vdots \\ \mathbf{0} & \ddots & \ddots & \ddots & \mathbf{0} \\ \vdots & \mathbf{0} & a_{n-1,1} & a_{n-1,2} & a_{n-1,3} \\ \mathbf{0} & \dots & \mathbf{0} & a_{n,1} & a_{n,2} \end{bmatrix} \begin{bmatrix} \partial(\vec{q}_1) \\ \partial(\vec{q}_2) \\ \vdots \\ \partial(\vec{q}_{n-1}) \\ \partial(\vec{q}_n) \end{bmatrix} = \begin{bmatrix} r(\vec{q}_1) \\ r(\vec{q}_2) \\ \vdots \\ r(\vec{q}_{n-1}) \\ r(\vec{q}_n) \end{bmatrix} \tag{12}$$

(13)

where,

$$a_{i,1} = \frac{\partial}{\partial \vec{q}_{i-1}} r(\vec{q}_i) \tag{14}$$

$$a_{i,2} = \frac{\partial}{\partial \vec{q}_i} r(\vec{q}_i) \tag{15}$$

$$a_{i,3} = \frac{\partial}{\partial \vec{q}_{i+1}} r(\vec{q}_i) \tag{16}$$

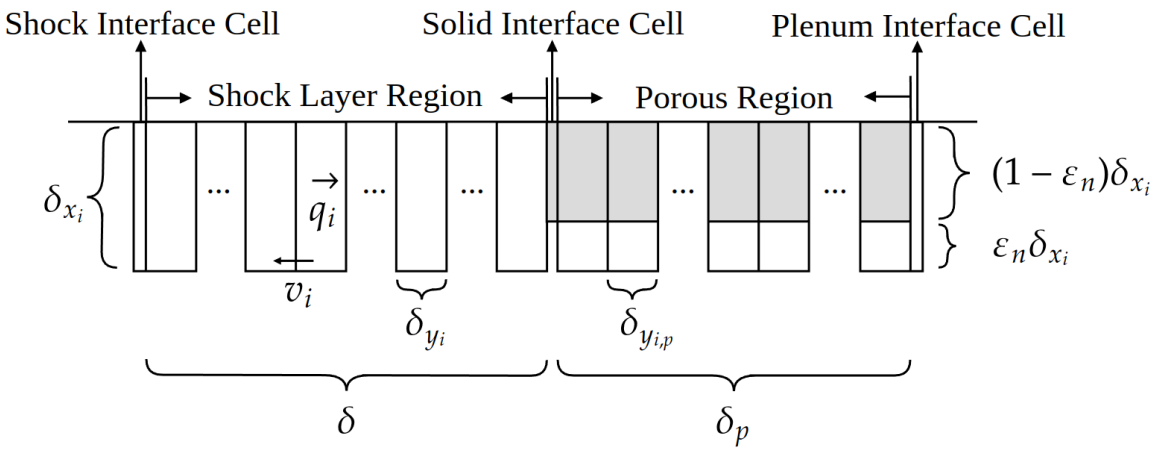

Fig. 6 Unified domain using staggered grid for numerical method

The presence of interfaces, however, necessitates the solution of additional equations. The first interface is introduced by the shock. The shock standoff distance is required to accurately represent the shape of the shock. This has the effect of introducing an additional equation to the system, defined by matching the normal velocity in the first post-shock cell to the post-shock velocity condition defined by the Rankine-Hugoniot relations. The second interface is defined at the wall and separates the boundary layer flow conditions from the restricted porous flow conditions. In order to represent discontinuous behavior at the interface, a no-height solid cell is used to carry fluxes between the last fluid cell and solid portion of the first porous cell as well as enforce interface conditions. The resulting equation added to the system generates an additional dependency for the adjacent cells on either side of the interface. This cell would therefore disrupt the tridiagonal scheme, requiring 5 diagonals due to the dependence of the surrounding cells on three additional cells, instead of two. Schur complements allow for the solution of additional equations introduced by interfaces, and therefore provide a computationally inexpensive mechanism for the resolution of the second complication. Thus, the resulting system of equations can be expressed using a block tridiagonal Jacobian matrix coupled with a Schur complement scheme to handle the two interfaces, which represents the system solved in this study.

$$\left[\begin{array}{cccccc|cc}
a_{1,2} & a_{1,3} & \mathbf{0} & & \dots & \mathbf{0} & s3_{\delta,1} & \mathbf{0} \\
a_{2,1} & a_{2,2} & a_{2,3} & \mathbf{0} & & \vdots & s3_{\delta,2} & \vdots \\
 & \ddots & \ddots & \ddots & & & \vdots & \mathbf{0} \\
\mathbf{0} & a_{int-1,1} & a_{int-1,2} & a_{int-1,3} & \mathbf{0} & & s3_{\delta,int-1} & s3_{int,int-1} \\
 & \mathbf{0} & a_{int+1,1} & 2_{int+1,2} & a_{int+1,3} & \mathbf{0} & s3_{\delta,int+1} & s3_{int,int+1} \\
 & & & \ddots & \ddots & \ddots & \vdots & \mathbf{0} \\
\vdots & & \mathbf{0} & a_{n-1,1} & a_{n-1,2} & a_{n-1,3} & s3_{\delta,n-1} & \vdots \\
\mathbf{0} & \dots & & \mathbf{0} & a_{n,1} & a_{n,2} & s3_{\delta,n} & \mathbf{0} \\
\hline
\mathbf{0} & \dots & & & s1_{n-1,\delta} & s1_{n,\delta} & \mathbf{0} & \mathbf{0} \\
\mathbf{0} & \dots & s1_{int-1,int} & s1_{int+1,int} & \dots & \mathbf{0} & s2_{\delta,int} & s2_{int,int}
\end{array}\right]
\left[\begin{array}{c}
\partial(\vec{q}_1) \\
\partial(\vec{q}_2) \\
\vdots \\
\partial(\vec{q}_{n-1}) \\
\partial(\vec{q}_n) \\
\partial\left(\begin{bmatrix} \delta \\ \vec{q}_{int} \end{bmatrix}\right)
\end{array}\right]
=
\left[\begin{array}{c}
r(\vec{q}_1) \\
r(\vec{q}_2) \\
\vdots \\
r(\vec{q}_{n-1}) \\
r(\vec{q}_n) \\
r\left(\begin{bmatrix} \delta \\ \vec{q}_{int} \end{bmatrix}\right)
\end{array}\right] \tag{17}$$

where,

$$s1_{i,int} = \frac{\partial}{\partial \vec{q}_i} r(\vec{q}_{int}) \tag{18}$$

$$s3_{\delta,i} = \frac{\partial}{\partial \delta} r(\vec{q}_i) \tag{19}$$

$$s3_{int,i} = \frac{\partial}{\partial \vec{q}_{int}} r(\vec{q}_i) \tag{20}$$

$$s2_{\delta,int} = \frac{\partial}{\partial \delta} r(\vec{q}_{int}) \tag{21}$$

$$s2_{int,int} = \frac{\partial}{\partial \vec{q}_{int}} r(\vec{q}_{int}) \tag{22}$$

It should be noted that $s1_{n-1,\delta}$ and $s1_{n,\delta}$ are populated with the boundary condition that the far-field normal velocity and post-shock velocity are equal, where cell $n+1$ is a no-height cell describing the post-shock conditions.

III. Validation

To validate the stagnation line solver, results in 11-species air for a Mach 7 test case were compared against the Yoshikawa correlation [29] and experimental data from Naved et. al [30], from which the specific test parameters and material properties were taken. The blowing ratio, F, normalizes the injected mass flux against the freestream mass flux.

$$F = \frac{\rho_{inj} u_{inj}}{\rho_\infty u_\infty} \tag{23}$$

The heat transfer Stanton number, St, is the convective heat flux, $\dot{q}_w$ normalized by the external flow enthalpy flux.

$$B_h = \frac{F}{St_{h0}} \tag{24}$$

$$St_h = \frac{\dot{q}_w}{\rho_\infty u_\infty (H_0 - h_w)} \tag{25}$$

$$H_0 = h_\infty + \frac{1}{2} u_\infty^2 \tag{26}$$

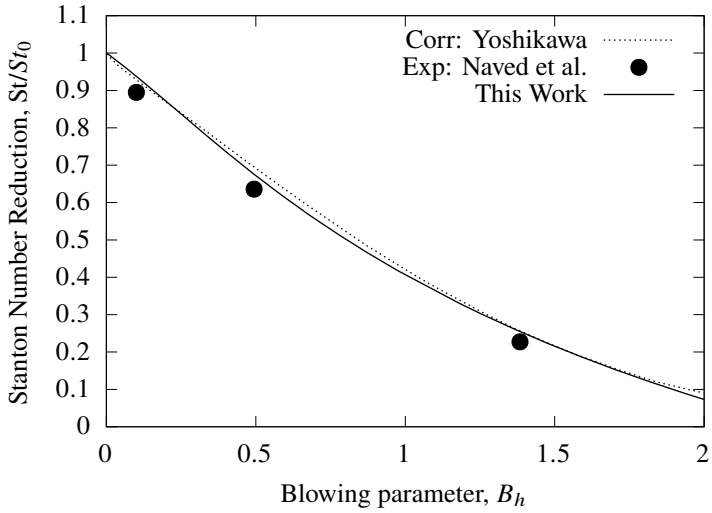

Fig. 7 Stanton number reduction versus blowing ratio for air with test conditions and material properties from Naved et al. [30]

When Stanton number and blowing ratio are normalized by the non-blowing Stanton number, St_0, they provide a useful description of cooling effectiveness. Figure 7 displays the results of the validation. The numerical results of this work align very nicely with both the correlation and experimental results. Thus, the solver appears applicable to 11-species air for hypersonic flight test cases in the equilibrium regime. Unfortunately, experimental data, and therefore empirical correlations, have not yet been published in a form that would allow for the validation of this solver

in the non-equilibrium regime. However, the validation of the two-temperature thermochemical model alongside the validation of the solver in equilibrium gives some confidence in the solver's applicability to non-equilibrium flight test cases. Ideally, future experimental test campaigns will provide Stanton number reduction plots or surface temperature reduction plots for non-equilibrium scenarios with which the solver can be further validated.

IV. Results

Results have been obtained for various injectants across a range of injectant blowing ratios. A specific case has been investigated that represents a generic hypersonic mission profile point relevant to transpiration cooling implementations. The test case is taken from validation material properties for porous alumina [30], and an altitude and freestream velocity of 40km and 4 km/s are chosen. Shock standoff distance for this condition is less than 10% of the nose tip radius (25 mm for the selected case). Given the standoff distance and post-shock velocity relevant to this case, non-equilibrium thermochemistry must be considered within the shock layer. However, temperatures remain low enough to avoid appreciable rates of ionization for all species.

Detailed profiles for the surface temperature and surface mass fraction of atomic oxygen are presented in Figures 8 and 9. The surface mass fraction is defined as the percentage of oxygen by mass relative to the fluid solution. While for this case the mass fraction never exceeds roughly 0.1, or 10%, even very small proportions of oxygen can result in surface recombination. Future results should report the proportion of stagnation heat flux for which surface oxidation reactions are responsible. As expected, helium outperforms argon and nitrogen for surface temperature reduction. This trend extends to the inhibition of species transport to the surface, likely related to the much lower molecular weight of helium. Figure 10 displays surface temperature reduction and concentration reduction across the three injectant candidates. While argon and nitrogren exhibit similar performance for surface transport of oxygen, the use of nitrogen results in a lower surface temperature and atomic oxygen mass fraction across all blowing ratios. Some numerical artifacts exist but do not take away from the general trends. The temperature dip just inside the porous medium for the 5% blowing case with nitrogen is likely the result of non-uniform refinement and an over-simplified numerical scheme to enforce upwinding that was not appropriately implemented for non-uniform grid spacing. Figures 11 and 12 display the full species profiles and temperature profiles, respectively, for a low and high blowing case. For these tests, nitrogen was employed as the injectant for the the flight conditions used throughout the study. The presence of local thermal non-equilibrium is displayed in Figure 12, where relaxation from the frozen post shock condition takes place across the shock layer. For the high blowing case, the interaction at the surface results in an increase in the vibrational modes of the fluid, increasing the solid temperature relative to the translational temperature. This is possibly the result of forced recombination at the surface and within the porous medium and will be studied in more detail in future work.

V. Conclusions and Future Work

Results from this study present the sensitivity of stagnation surface temperature and surface composition relative to a specific flight altitude and speed for several coolant injectant rates and compositions. The differences in performance have implications for one of the biggest challenges to the implementation of transpiration cooling: infrastructure for coolant storage. The possible use of light gases, gases already being carried by the vehicle, or gases claimed from exhaust as a suitable coolant might reduce the space and weight required for a transpiration cooling application. While the results presented here are limited in scope, some design choice conclusions can be drawn. For more traditional surface materials limited by melting temperature, helium would likely be the appropriate choice. Similarly, for materials limited by the onset of oxidation as opposed to melting temperature, such as Ultra-High Temperature Composites, helium provides better protection. In should be noted that in providing results with blowing ratios, the difference in molecular weights is emphasized. Future studies should aim to present Stanton number reduction versus blowing parameter to better assess the relative benefits of injectant candidates.

Further, the above results present detailed profiles of surface temperature and species compositions through the stagnation line for a selected case that represents realistic flight characteristics. These results can be extended to a variety of test cases for example engineering calculations for possible vehicle designs, allowing for conclusions on the possible coolant consumption for various missions. Studying performance relative to porous medium thickness could provide useful design information for plenum conditions. The capability to formulate these results quickly demonstrates the utility of the presented work as a tool for the iterative design of real hypersonic vehicles.

Future efforts hope to expand on several aspects of the solver, while maintaining low computational cost. Most globally, examples calculations for generic vehicle geometries could be attained, displaying the direct utility to vehicle

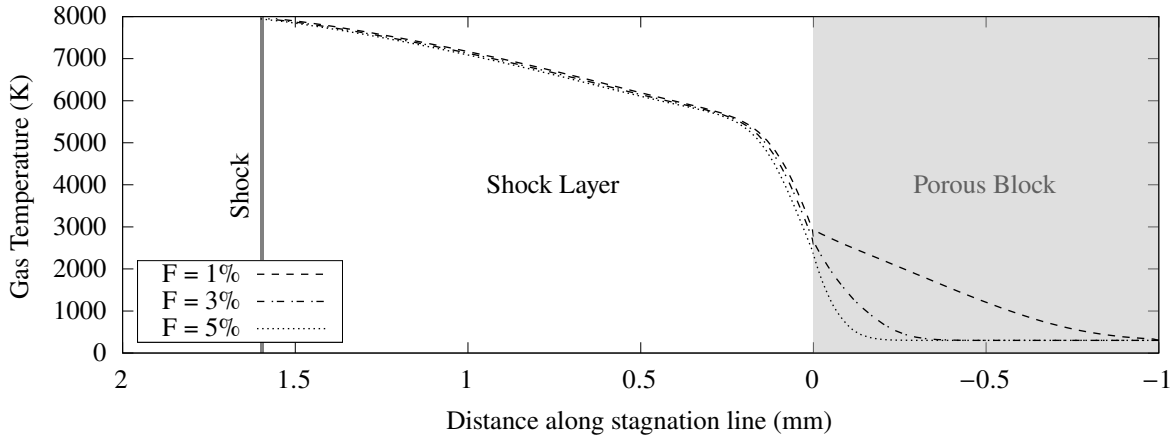

(a) Argon

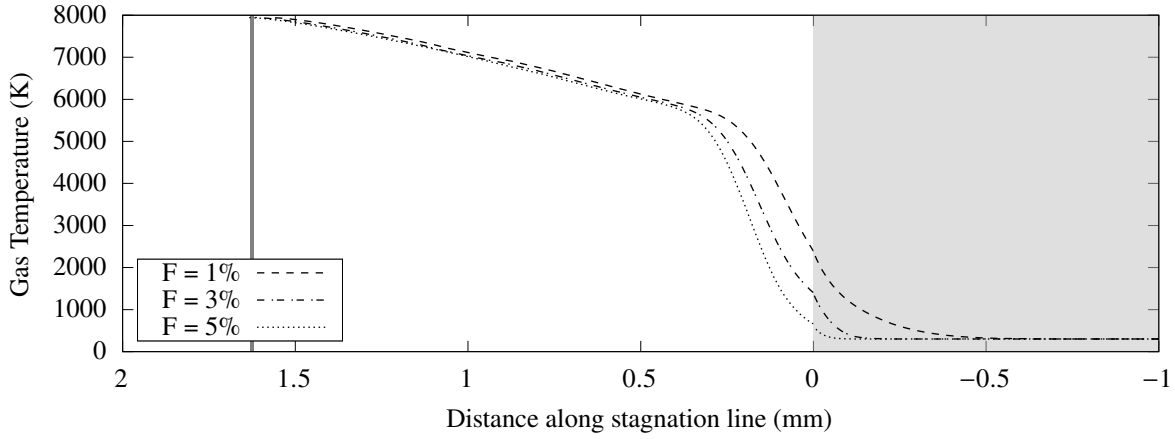

(b) Helium

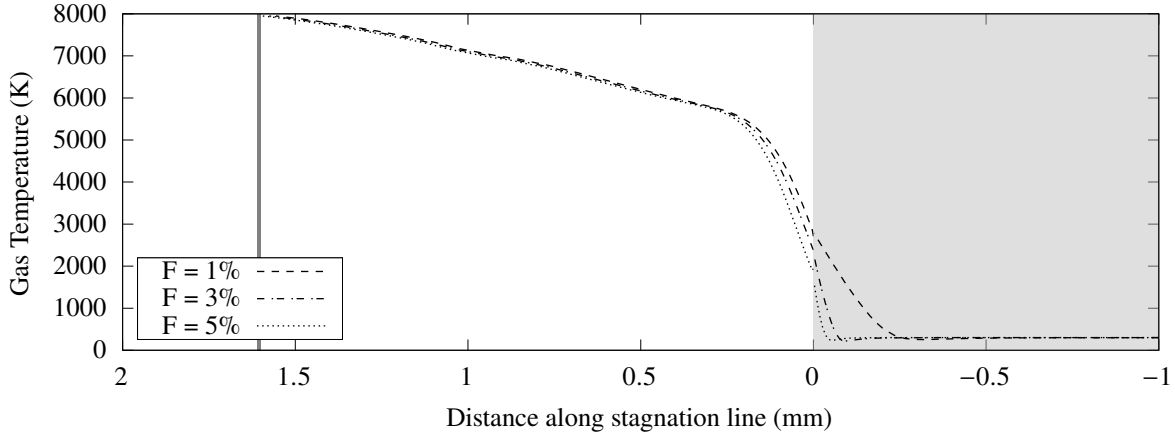

(c) Nitrogen

Fig. 8 Temperature profiles for varying blowing ratio and injectant

designers. More specifically, significant improvements can be made to the treatment of the porous medium and the interface. Grid refinement on the order of pore size would necessarily require the solver be adapted into two dimensions. However, extension to more complex geometries, while requiring more complex tangential boundary treatment, would not necessarily require the adoption of a two dimensional framework. These geometries could be used to model swept

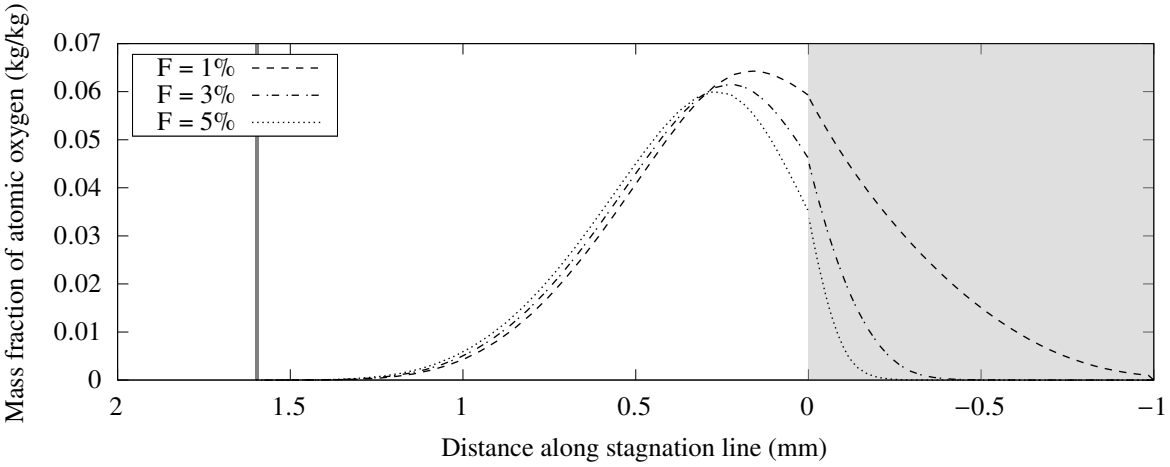

(a) Argon

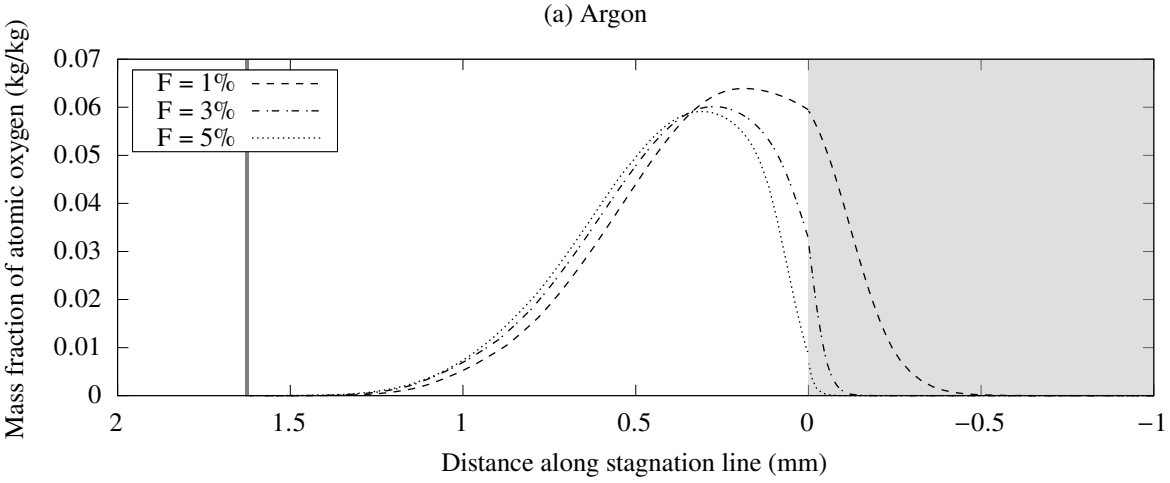

(b) Helium

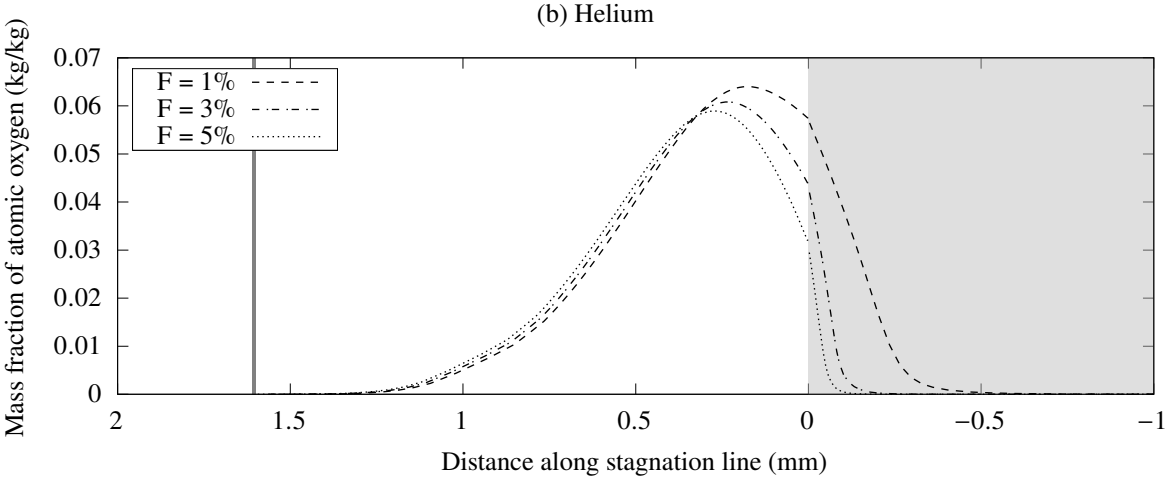

(c) Nitrogen

Fig. 9 Atomic oxygen concentration profiles for varying blowing ratio and injectant

leading edges which would offer a more robust path toward modeling mission heat load for an entire geometry. Oxidation and ablation could be incorporated efficiently, as the entire porous medium is already modelled and could be recessed for an ablation case. The ability to resolve the entire domain could be useful in creating efficient ablative model that handles recession by resolving surface conditions from the previous profiles. Lastly, future study should incorporate

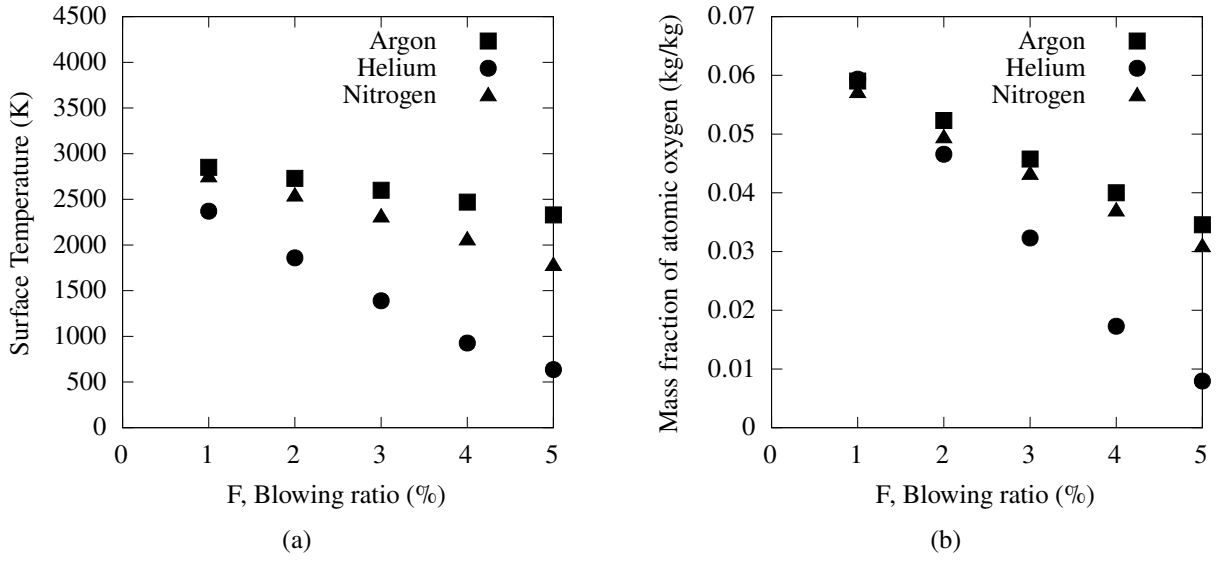

Fig. 10 Surface temperature (a) and concentration of atomic oxygen (b) relative to blowing ratio

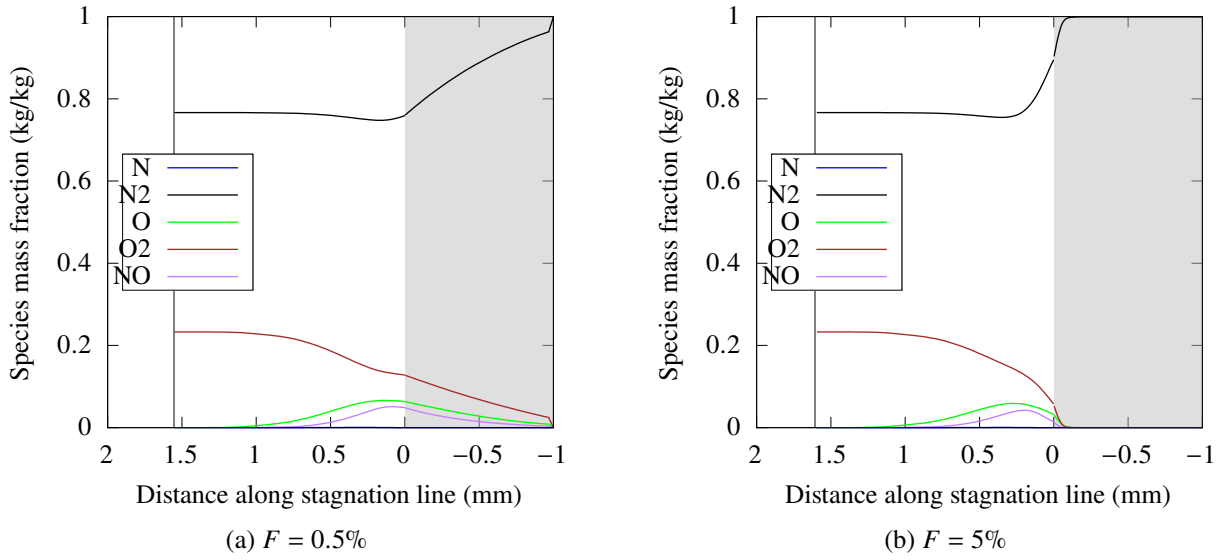

Fig. 11 Full species profiles for nitrogen injectant at low and high blowing

more complex injectants. The consideration of reducing atmosphere injectants could provide useful information on the performance of injectants derived from fuel sources already carried by hypersonic vehicles. The solver presented in this study thus provides a useful starting point for a variety of investigations.

Appendix

A. Chemical Model Reactions and Rates

Acknowledgments

Samuel Brody gratefully acknowledges the Marshall Commission for financial support as well as the U.S. Air Force for their support of this effort. Justin Clarke gratefully acknowledges the Rhodes Trust for financial support.

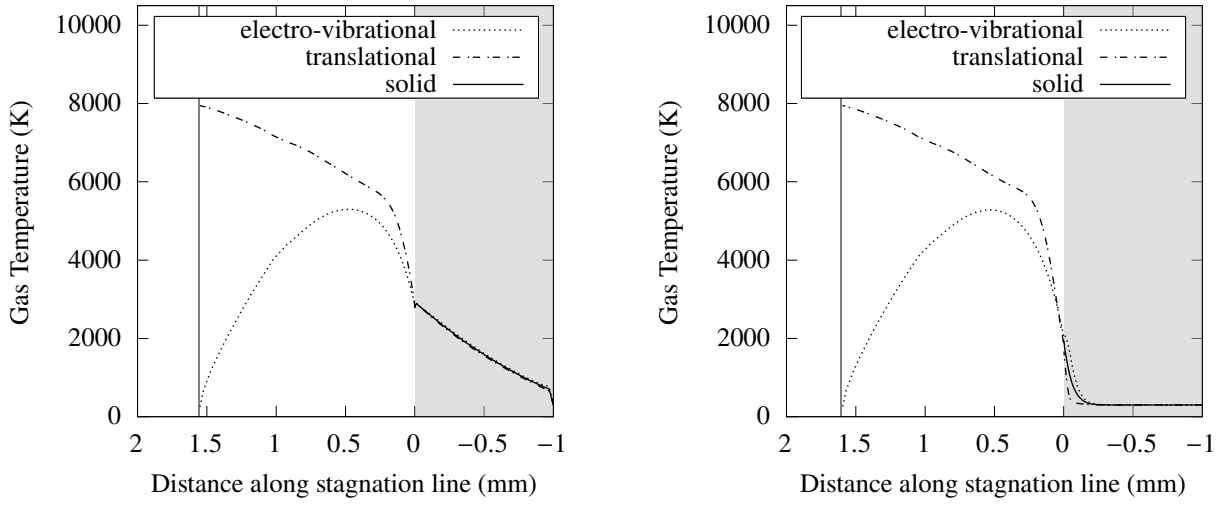

(a) $F = 0.5\%$ (b) $F = 5\%$

Fig. 12 Translational, electro-vibrational, and solid temperature profiles for nitrogen injectant at low and high blowing

References

[1] Ewenz Rocher, M., Hermann, T., McGilvray, M., Grossman, M., and Vandeperre, L., "Measuring the Concentration of Freestream Species on a Hypersonic Transpiration-Cooled Stagnation Point," *Journal of Spacecraft and Rockets*, Vol. 59, No. 4, 2022, pp. 1380–1387.

[2] Ravichandran, R., Doherty, L. J., McGilvray, M., Damm, K., and Gollan, R., *Aerodynamic Effects and Heat Flux Augmentation of a Transpiration Cooled Hypersonic Sharp Leading Edge*, 2023.

[3] Blottner, F., "Viscous Shock layer at the Stagnation Point with Nonequilibrium Air Chemistry," *AIAA Journal*, Vol. 7, 1969, pp. 2281–2288.

[4] Cheng, H., "The Blunt-Body Problem in Hypersonic Flow at Low Reynolds Numbers," , No. AF-1285-A-10, 1963.

[5] Gnoffo, P. A., Gupta, R. N., and Shinn, J. L., "Conservation equations and physical models for hypersonic air flows in thermal and chemical nonequilibrium," Tech. Rep. NASA TP 2867, 1989.

[6] Clarke, J., Di Mare, L., and McGilvray, M., "Quasi One-Dimensional Non-Equilibrium Shock Tube Solver," *Submitted to AIAA Journal*, 2024.

[7] Cimolin, F., and Discacciati, M., "Navier–Stokes/Forchheimer models for filtration through porous media," *Applied Numerical Mathematics*, Vol. 72, 2013, pp. 205–224.

[8] Erugn, S., "Fluid Flow through Packed Columns," *Chemical Engineering Progress*, Vol. 48, 1952, pp. 89–94.

[9] Hermann, T. A., McGilvray, M., Ifti, H. S., Hufgard, F., and Loehle, S., *Fluid-Solid Heat Exchange in Porous Media for Transpiration Cooling Systems*, 2023.

[10] Homann, F., "Einfluß großer zähigkeit bei strömung um zylinder," *Forschung auf dem Gebiet des Ingenieurwesens A*, Vol. 7, No. 1, 1936, pp. 1–10.

[11] Herring, T. K., "The boundary layer near the stagnation point in hypersonic flow past a sphere," *Journal of Fluid Mechanics*, Vol. 7, 1960, pp. 257–272.

[12] Fay, J. A., and Riddell, F. R., "Theory of Stagnation Point Heat Transfer in Dissociated Air," *Journal of the Aerospace Sciences*, Vol. 25, No. 2, 1958, pp. 73–85.

[13] Clarke, J., Collen, P. L., McGilvray, M., and di Mare, L., "Numerical Simulation of a Shock Tube in Thermochemical Non-Equilibrium," *AIAA SCITECH 2023 Forum*, 2023.

Table 1 Chemical Reactions from Gupta *et al.* [19] with inert gas ionization

Reaction Number	Reaction	Third body M
	Dissociation	
1	$O_2 + M_1 \rightleftharpoons 2\,O + M_1$	O, N, O_2, N_2, NO
2	$N_2 + M_2 \rightleftharpoons 2\,N + M_2$	O, O_2, N_2, NO
3	$N_2 + N \rightleftharpoons 2\,N + N$	
4	$NO + M_3 \rightleftharpoons N + O + M_3$	O, N, O_2, N_2, NO
5	$NO + O \rightleftharpoons O_2 + N$	
6	$N_2 + O \rightleftharpoons NO + N$	
	Oxidation	
7	$N + O \rightleftharpoons NO^+ + e^-$	
8	$O + e^- \rightleftharpoons O^+ + e^- + e^-$	
9	$N + e^- \rightleftharpoons N^+ + e^- + e^-$	
10	$O + O \rightleftharpoons {O_2}^+ + e^-$	
11	$NO + M_4 \rightleftharpoons NO^+ + e^- + M_4$	O_2, N_2
	Redox	
12	$O + {O_2}^+ \rightleftharpoons O_2 + O^+$	
13	$N_2 + N^+ \rightleftharpoons N + {N_2}^+$	
14	$N + N \rightleftharpoons {N_2}^+ + e^-$	
15	$O_2 + N_2 \rightleftharpoons NO + NO^+ + e^-$	
16	$O + NO^+ \rightleftharpoons NO + O^+$	
17	$N_2 + O^+ \rightleftharpoons O + {N_2}^+$	
18	$N + NO^+ \rightleftharpoons NO + N^+$	
19	$O_2 + NO^+ \rightleftharpoons NO + {O_2}^+$	
20	$O + NO^+ \rightleftharpoons O_2 + N^+$	
	Inert gas ionization	
21	$Ar + e^- \rightleftharpoons Ar^+ + e^- + e^-$	
22	$He + e^- \rightleftharpoons He^+ + e^- + e^-$	

[14] Parthasarathy, T., Rapp, R., Opeka, M., and Kerans, R., "A model for the oxidation of ZrB2, HfB2 and TiB2," *Acta Materialia*, Vol. 55, No. 17, 2007, pp. 5999–6010.

[15] Scott, C. D., Periaux, J., and Ballmann, J., *Wall Catalytic Recombination and Boundary Conditions in Nonequilibrium Hypersonic Flows — with Applications*, Birkhäuser Boston, Boston, MA, 1992, pp. 176–250.

[16] Park, C., *Nonequilbrium Hypersonic Aerothermodynamics*, John Wiley & Sons, Inc., 1990.

[17] Hirschfelder, J. O., Curtiss, C. F., and Bird, R. B., *Molecular Theory of Gases and Liquids*, John Wiley & Sons, Inc., 1954.

[18] Yos, J. M., "Transport properties of nitrogen, hydrogen, oxygen, and air to 30,000 K," Tech. Rep. RAD-TM-63-7, AVCO CORP WILMINGTON MA RESEARCH AND ADVANCED DEVELOPMENT DIV, 1963.

[19] Gupta, R. N., Yos, J. M., and Thompson, R. A., "A review of reaction rates and thermodynamic and transport properties for the 11-species air model for chemical and thermal nonequilibrium calculations to 30000 K," Tech. Rep. NASA RP-1232, NASA, 1989.

[20] Wilke, C. R., "A viscosity equation for gas mixtures," *The Journal of Chemical Physics*, Vol. 18, No. 4, 1950, pp. 517–519.

Table 2 Chemical Reaction Rate Coefficients from Gupta *et al.* [19] with inert gas ionization

Reaction	Forward rate coefficients $k_{f,r} = A_{f,r} T^{\alpha_{f,r}} e^{-T_{f,r}/T_{av}}$			Backward rate coefficients $k_{b,r} = A_{b,r} T^{\alpha_{b,r}} e^{-T_{b,r}/T}$		
	$A_{f,r}$	$\alpha_{f,r}$	$T_{f,r}$	$A_{b,r}$	$\alpha_{b,r}$	$T_{b,r}$
1	3.61×10^{18}	−1.0	5.94×10^{4}	3.01×10^{15}	−0.5	0.0
2	1.92×10^{17}	−0.5	1.131×10^{5}	1.09×10^{16}	−0.5	0.0
3	4.15×10^{22}	−1.5	1.131×10^{5}	2.32×10^{21}	−1.5	0.0
4	3.97×10^{20}	−1.5	7.56×10^{4}	1.01×10^{20}	−1.5	0.0
5	3.18×10^{9}	1.0	1.97×10^{4}	9.63×10^{11}	0.5	3.6×10^{3}
6	6.75×10^{13}	0.0	3.75×10^{4}	1.5×10^{13}	0.0	0.0
7	9.03×10^{9}	0.5	3.24×10^{4}	1.80×10^{19}	−1.0	0.0
8	$(3.6 \pm 1.2) \times 10^{31}$	−2.91	1.58×10^{5}	$(2.2 \pm 0.7) \times 10^{40}$	−4.5	0.0
9	$(1.1 \pm 0.4) \times 10^{32}$	−3.14	1.69×10^{5}	$(2.2 \pm 0.7) \times 10^{40}$	−4.5	0.0
10	$(1.6 \pm 0.4) \times 10^{17}$	−0.98	8.08×10^{4}	$(8.02 \pm 2.0) \times 10^{21}$	−1.5	0.0
11	2.2×10^{15}	−0.35	1.08×10^{5}	2.2×10^{26}	−2.5	0.0
12	2.92×10^{18}	−1.11	2.8×10^{4}	7.8×10^{11}	0.5	0.0
13	2.02×10^{11}	0.81	1.3×10^{4}	7.8×10^{11}	0.5	0.0
14	$(1.4 \pm 0.3) \times 10^{13}$	0.0	6.78×10^{4}	$(1.5 \pm 0.5) \times 10^{22}$	−1.5	0.0
15	1.38×10^{20}	−1.84	1.41×10^{5}	1.0×10^{24}	−2.5	0.0
16	3.63×10^{15}	−0.6	5.08×10^{4}	1.5×10^{13}	0.0	0.0
17	3.4×10^{19}	−2.0	2.3×10^{4}	2.48×10^{19}	−2.2	0.0
18	1.0×10^{19}	−0.93	6.1×10^{4}	4.8×10^{14}	0.0	0.0
19	1.8×10^{15}	−0.17	3.3×10^{4}	1.8×10^{13}	0.5	0.0
20	1.34×10^{13}	−0.31	7.727×10^{4}	1.0×10^{14}	0.0	0.0
21 [31]	2.5×10^{34}	−3.82	1.817×10^{5}			
22 [32]	3.33×10^{20}	0.5	2.852×10^{5}			

[21] Gordon, S., and McBride, B. J., "Computer Program for Calculation of Complex Chemical Equilibrium," Tech. Rep. NASA-RP-1311, 1994.

[22] Palmer, G. E., and Wright, M. J., "Comparison of methods to compute high-temperature gas viscosity," *Journal of Thermophysics and Heat Transfer*, Vol. 17, 2003, pp. 232–239.

[23] Muckenfuss, C., and Curtiss, C. F., "Thermal conductivity of multicomponent gas mixtures," *The Journal of Chemical Physics*, Vol. 29, 1958, pp. 1273–1277.

[24] Capitelli, M., Colonna, G., Gorse, C., and D'angola, A., "Transport properties of high temperature air in local thermodynamic equilibrium," *The European Physical Journal D - Atomic, Molecular, Optical and Plasma Physics*, Vol. 11, 2000, pp. 279–289.

[25] Murphy, A. B., and Arundell, C. J., "Transport Coefficients of Argon, Nitrogen, Oxygen, Argon-Nitrogen, and Argon-Oxygen Plasmas," *Plasma Chemistry and Plasma Processing*, Vol. 14, 1994.

[26] Murphy, A. B., "Transport Coefficients of Air, Argon-Air, Nitrogen-Air, and Oxygen-Air Plasmas," *Plasma Chemistry and Plasma Processing*, Vol. 15, 1995.

[27] Moss, J. N., "Reacting Viscous-Shock-Layer Solutions with Multicomponent Diffusion and Mass Injection," Tech. Rep. NASA-TR-R-411, 1974.

[28] Harlow, F. H., and Welch, J. E., "Numerical Calculation of Time-Dependent Viscous Incompressible Flow of Fluid with Free Surface," *The Physics of Fluids*, Vol. 8, No. 12, 1965, pp. 2182–2189.

[29] Yoshikawa, K. K., "Linearized Theory of Stagnation Point Heat and Mass Transfer at Hypersonic Speeds," Tech. Rep. NASA TN D-5246, 1969.

[30] Naved, I., Hermann, T., McGilvray, M., Ewenz Rocher, M., Hambidge, C., Doherty, L., Le Page, L., Grossman, M., and Vandeperre, L., "Heat Transfer Measurements of a Transpiration-Cooled Stagnation Point in Transient Hypersonic Flow," *Journal of Thermophysics and Heat Transfer*, Vol. 37, No. 2, 2023, pp. 296–308.

[31] Gokcen, T., "N2-CH4-Ar Chemical Kinetic Model for Simulations of Atmospheric Entry to Titan," *Journal of Thermophysics and Heat Transfer*, Vol. 21, No. 1, 2007, pp. 9–18.

[32] Leibowitz, L. P., and Kuo, T.-J., "Ionizational Nonequilibrium Heating During Outer Planetary Entries," *AIAA Journal*, Vol. 14, No. 9, 1976, pp. 1324–1329.